
This is an electronic reprint of the original article.
This reprint may differ from the original in pagination and typographic detail.

Moriam, Kaniz; Sawada, Daisuke; Nieminen, Kaarlo; Ma, Yibo; Rissanen, Marja; Nygren, Nicole; Guizani, Chamseddine; Hummel, Michael; Sixta, Herbert

Spinneret geometry modulates the mechanical properties of man-made cellulose fibers

Published in:
Cellulose

DOI:
[10.1007/s10570-021-04220-y](https://doi.org/10.1007/s10570-021-04220-y)

Published: 01/11/2021

Document Version
Publisher's PDF, also known as Version of record

Published under the following license:
CC BY

Please cite the original version:
Moriam, K., Sawada, D., Nieminen, K., Ma, Y., Rissanen, M., Nygren, N., Guizani, C., Hummel, M., & Sixta, H. (2021). Spinneret geometry modulates the mechanical properties of man-made cellulose fibers. *Cellulose*, 28(17), 11165-11181. <https://doi.org/10.1007/s10570-021-04220-y>

This material is protected by copyright and other intellectual property rights, and duplication or sale of all or part of any of the repository collections is not permitted, except that material may be duplicated by you for your research use or educational purposes in electronic or print form. You must obtain permission for any other use. Electronic or print copies may not be offered, whether for sale or otherwise to anyone who is not an authorised user.



Spinneret geometry modulates the mechanical properties of man-made cellulose fibers

Kaniz Moriam · Daisuke Sawada · Kaarlo Nieminen · Yibo Ma ·
Marja Rissanen · Nicole Nygren · Chamseddine Guizani · Michael Hummel ·
Herbert Sixta 

Received: 4 August 2021 / Accepted: 17 September 2021 / Published online: 7 October 2021
© The Author(s) 2021

Abstract The production of cellulose-based textile fibers with high toughness is vital for extending the longevity and thus developing a sustainable textile industry by reducing the global burden of microplastics. This study presented strategies to improve fiber toughness by tuning spinneret geometries. Experimental studies were conducted by spinning with different spinneret geometries and measuring the mechanical and structural properties of the spun fibers. In addition, numerical simulation tools were used to

better understand the effects of spinneret geometry. The altering parameters of the spinneret geometries were the capillary diameters D , the angle of the entry cone into the spinning capillary, and the ratio of capillary length to diameter L/D . The highest fiber toughness could be achieved at a capillary aspect ratio of 1 to 2. The obtained maximum fiber toughness was 93 MPa with a tensile strength of 60 cN/tex and a concomitant elongation of 16.5%. For these fiber properties, a 13 wt% solution of a high-purity pulp with higher viscosity in [DBNH][OAc] was spun into a 1.3 dtex fiber using a D100 spinneret with a capillary of 1:1 length/diameter and an entrance angle of 8° . It

Supplementary Information The online version contains supplementary material available at <https://doi.org/10.1007/s10570-021-04220-y>.

K. Moriam · D. Sawada · K. Nieminen ·
Y. Ma · M. Rissanen · N. Nygren ·
C. Guizani · M. Hummel · H. Sixta (✉)
Department of Bioproducts and Biosystems, School of
Chemical Engineering, Aalto University, P.O Box 16300,
00076 Espoo, Aalto, Finland
e-mail: herbert.sixta@aalto.fi

K. Moriam
e-mail: most.moriam@aalto.fi

D. Sawada
e-mail: daisuke.sawada@aalto.fi

K. Nieminen
e-mail: kaarlo.nieminen@aalto.fi

Y. Ma
e-mail: yibo.ma@aalto.fi

M. Rissanen
e-mail: marja.rissanen@aalto.fi

N. Nygren
e-mail: nicole.nygren@aalto.fi

C. Guizani
e-mail: chamseddine.guizani@aalto.fi

M. Hummel
e-mail: michael.hummel@aalto.fi

was noticeable that the microvoid orientations decreased almost linearly with increasing toughness of the fibers. The morphologies of the fibers were similar regardless of the spinneret geometries and the raw materials used in the spinning process. In summary, by modulating the spinneret geometries, Ioncell fibers obtained high toughness that have the potential to replace synthetic fibers.

Keywords Man-made cellulose fibers · Toughness of cellulose fiber · Spinneret geometry · Capillary aspect ratio of spinneret · Ionic liquid · Ioncell Technology · Dry-jet wet spinning

Introduction

Synthetic textiles dominate global textile production due to their low production cost. However, the unsustainable production processes for synthetic textiles, their lack of biodegradability and the resulting pollution by microplastic fibers are of global concern (Stone et al. 2020; Salvador et al. 2017; Royer et al. 2021). To promote the circular economy and sustainable textile production, synthetic textile should be gradually replaced by eco-friendly textiles. However, this implies that biodegradable textile fibers should have some properties that can currently only be achieved using synthetic fibers.

Man-made cellulose fibers produced from wood pulp derived from sustainable forestry or other ligno-cellulosic raw materials are more sustainable than synthetic fibers and cotton (Shen et al. 2010; Moriam et al. 2021a). With the development of lyocell fiber technology, a much more sustainable technology is now available to produce high-quality textiles compared to the viscose process (Sayyed et al. 2019b, 2019a; Jiang et al. 2020). Additionally, lyocell fiber technology also has the potential to upcycle cellulose-based waste textiles (Haslinger et al. 2019a, b; Wedin et al. 2019; Ma et al. 2018a, b), especially those made of natural cellulose fibers or viscose, into higher added value textile fibers.

The high toughness of cellulose-based textile fibers enables the development of sustainable textiles and upcycling of cellulosic waste textiles into durable textile fibers. However, commercially available high tenacity cellulose fibers compromise the good

elongation property and vice versa (Sixta et al. 2015). Hence, a simultaneous increase of elongation and tenacity properties is required to enhance the toughness (the integral over the tenacity-elongation curve).

Ioncell® technology is a recently developed lyocell process to produce man-made cellulosic fibers from ionic liquid solutions by dry-jet wet spinning (Sixta et al. 2015; Asaadi et al. 2016; Michud et al. 2015). Ioncell is an environmentally friendly process and considered as an alternative to the viscose and *N*-methylmorpholine *N*-oxide (NMMO)-based Lyocell processes (Michud et al. 2015; Elsayed et al. 2020). The ionic liquid ‘1,5-diazabicyclo [4.3.0] non-5-ene acetate [DBNH][OAc]’ is used as an excellent cellulose solvent allowing for a rapid dissolution at moderate temperatures and subsequent shaping into continuous filaments (Hummel et al. 2016). Highly orientated cellulose fibers with high tenacity are obtained by coagulation in a cold-water bath (Hauru et al. 2014).

The process parameters, including extrusion velocity, draw ratio, airgap, spinneret geometry, and coagulation bath temperature, considerably influence the mechanical properties of man-made cellulose fiber produced via lyocell process (Hauru et al. 2014; Michud et al. 2016). Michud et al. previously reported the effect of spinneret diameter (150 vs. 100 μm), draw ratio, and coagulation bath temperature on the structural and mechanical properties of the cellulose fiber (Michud et al. 2016). Guizani et al. presented the effect of air gap conditioning on the mechanical properties of the fibers using a monofilament spinning plant (Guizani et al. 2020b). Previously, two studies were performed to observe the effect of spinneret aspect ratio (L/D) on the Ioncell fiber properties. Hauru et al. reported that a L/D of 2 improved the Ioncell fiber orientation compared to a shorter L/D of 0.2 (Hauru et al. 2014). Later, Guizani et al. further justified that the increase in L/D leads to better mechanical properties of the spun fibers (Guizani et al. 2020a). However, both studies were done with a monofilament spinning system, which was only conditionally representative of real spinning conditions. Moreover, there is a lack of systematic knowledge about the geometry of the spinneret capillaries, such as the length-to-diameter ratio of the capillary, the entrance cone geometry, and the use of multi-hole spinnerets.

Spinneret geometry is one of the important spinning parameters that affects the spinnability, the structural properties, and the fiber mechanical properties (Michud et al. 2016; Wang et al. 2018). The influence of the spinneret diameter on the mechanical properties of the NMMO- Lyocell fibers was investigated. Mortimer et al. reported that the narrower the spinneret, the shorter the draw length. In addition, the die swell effect is smaller for the spinneret with holes of a lower diameter due to the efficient cooling (Mortimer and Péguy 1995).

The effect of the spinneret geometry in the solution flow during spinning was investigated rigorously in a series of publications by Xia et al. for the dry-jet wet spinning of the cellulose/1-butyl-3-methylimidazolium [BMIM]CL solution (Xia et al. 2014, 2015, 2016). Xia et al. studied the effect of the entrance angle and the influence of the capillary length in the flow behavior of the spinning solution using numerical simulation (Xia et al. 2014). According to their study, longer spinneret aspect ratio helped to stabilize the viscosity of the cellulose/IL solution promoting the smooth solution flow. Furthermore, the study reported that the die swell effect was reduced by a shorter spinneret entrance angle and an increased length of the exit channel. A shorter entrance angle reduced the velocity gradient along the flow direction and a longer capillary length promoted the relaxation of the polymer chain. In addition, the longer capillary promoted a stable viscosity of the cellulose solution compared to the shorter capillary. The apparent viscosity remained stable due to the molecular orientation in the outlet channel.

Kirichenko et al. suggested the use of rectangular spinnerets instead of the circular spinnerets to reduce the irregularities of the diameter of the spun Capron yarn (Kirichenko et al. 1977). According to their study, the fluctuation of the airflow and the difference in heat transfer from the filaments to the air depend on the arrangement of the spinneret hole. The cooling conditions of the filaments were more uniform when the spinneret holes were arranged in straight lines compared to the concentric circles due to the transverse unilateral air flow. Due to the uniform cooling in the airgap, the rectangular arrangement of spinneret hole produced yarn that had more regularity in the yarn diameter.

We have previously shown that a longer capillary length of the spinneret for a given diameter

significantly increased the fiber toughness under otherwise identical spinning conditions (Moriama et al. 2021b). According to that study, Ioncell fiber achieved a modulus of toughness of 83.3 MPa, which presented the potential of Ioncell fibers to have higher strength and toughness than any other existing cellulose fibers. The long-term goal of the study was to reach the toughness of polyester fibers (128 MPa), a common synthetic textile fiber (Moriama et al. 2021b). As a continuation of the previous study, we have used different spinneret geometries with varying spinneret shape (circular to rectangular hole arrangement), entrance angle, spinneret diameter, hole number, and capillary length to observe their effects in mechanical properties in the final fiber. In addition, the influence of spinneret geometries on the solution flow was investigated using numerical simulation. Furthermore, we investigated the combined effect of the optimized spinneret geometry and different pulps (standard grade and high purity pulp) on the mechanical properties of the spun fibers. Finally, the structural properties of the high toughness fibers and their morphological properties were reported.

The effect of spinneret geometry in the spun fibers' mechanical properties has not been published before systematically for dry-jet wet spinning. This work will present new insight of improving toughness of man-made cellulose fibers toughness by tuning the spinneret geometries.

Experimental part

Raw materials

This study used high-purity pine pre-hydrolysis Kraft pulp additionally purified with cold caustic extraction produced by Georgia Pacific denoted as high purity grade pulp or HPG-pulp (intrinsic viscosity, CUEN, ISO 5351/1, of 594 ml/g; $M_n = 96.5$ kg/mol and $M_w = 209$ kg/mol, calculated by GPC-MALLS, hemicellulose 0.7%) and birch pre-hydrolysis Kraft pulp denoted as STG-pulp (Standard grade Pulp) (intrinsic viscosity 482 ml/g; $M_n = 49.3$ kg/mol and $M_w = 161.7$ kg/mol; hemicellulose 6.8%) (Moriama et al. 2021b). Equimolar amount of 1,5-diazabicyclo [4.3.0] non-5-ene (99% Fluorochem, UK) and acetic acid (100% Merck, Germany) were used to synthesize the Ionic liquid 1,5-diazabicyclo [4.3.0] non-5-ene acetate

[DBNH][OAc] for the dissolution of cellulose. Elmer GmbH, Austria provided 10 different spinneret geometries having rectangular hole distributions (Fig. S1) and, as a reference, the spinneret with circular hole distribution (Fig. S1) obtained from Enka Technica, Germany (Table 1).

Dope preparation and rheology

The grinded pulps were dissolved in melted [DBNH][OAc] for 90 min at 80 °C using a vertical kneader system. The cellulose concentration of the dope was 13–15 wt%. After dissolution, the dopes were filtered using a press filtration unit (metal filter fleece, absolute fineness of 5–6 μm). The rheological properties of the dopes were measured using the Anton Paar Physica MCR 302 rheometer containing parallel plate geometry (plate diameter 25 mm and gap size 1 mm). A dynamic sweep test ($100\text{--}0.1\text{ s}^{-1}$) was performed to record the complex viscosity and the dynamic moduli (G' and G''). Zero shear viscosity was calculated using a cross viscosity model (Michud et al. 2016) assuming the validity of the Cox-Merz rule.

Dry-jet wet spinning

Dry-jet wet spinning of the cellulose solutions (dopes) were performed using a customized laboratory piston spinning unit (Fourné Polymertechnik, Germany). The

molten dope was extruded through spinnerets. The filaments were coagulated in a water bath (8–10 °C) keeping an airgap of 1 cm and further guided by Teflon rollers to the godet (velocity varied from 5 to 95 m min^{-1} depending on the obtained draw ratios). The fibers were washed with hot water (80 °C) for 2 h under continuous magnetic stirring (the water was changed every 30 min). Fibers were air-dried after washing.

Numerical simulation

The velocity and shear rate distributions affecting the molecular alignment of the cellulose strands in the cellulose solutions were evaluated by simulating the flow of the cellulose solution using the COMSOL Multiphysics software using the Computational Fluid Dynamics module. Prior to this, the viscosity cross-model parameters were estimated from shear rate viscosity data of the dope by fitting the model to the experimental data using Wolfram Mathematica (Moriham et al. 2021b). Accordingly, the simulation of velocity and shear rate distributions in a spinneret channel was done in the Computational Fluid Dynamics module of COMSOL, assuming laminar flow and employing the fitted cross-model to describe the shear rate dependence of the viscosity. By virtue of the axisymmetric spinneret channels, it suffices to create a corresponding 2D geometry in which to carry out the simulation.

Table 1 The list of spinnerets

Name (Number of holes \times diameter \times aspect ratio)	L/D	Diameter (μm)	Hole number	Hole density (holes/ cm^2)	Entrance angle	Hole distribution (Fig. S1)
504 \times 100 \times 0.2	0.2	100	504	221	8°	Rectangular (Fig. S1)
504 \times 100 \times 1.0	1.0	100	504			
216 \times 100 \times 1.5	1.5	100	216	95		
216 \times 100 \times 2.0	2.0	100				
216 \times 100 \times 4.0	4.0	100				
216 \times 100 \times 5.0	5.0	100				
216 \times 80 \times 0.2	0.2	80				
216 \times 80 \times 1.0	1.0	80				
216 \times 50 \times 0.2	0.2	50				
216 \times 50 \times 1.0	1.0	50				
400 \times 100 \times 0.2	0.2	100	400	58	60°	Circular (Fig. S1)

In the simulation, the integration of the scalar product of the shear stress and shear rate over the channel geometry gives a quantity that summarizes the work per unit time accomplished by the shear forces on the viscous fluid in the channel- the shear power.

Considering an infinitesimal portion of the flow, we can conclude the shear power absorbed to be

$$dP = \sigma \cdot \dot{\gamma} dV. \quad (1)$$

Here dP is the (infinitesimal) power absorbed by the volume element dV whereas σ and $\dot{\gamma}$ are the shear stress and shear rate, respectively. Expressing the shear stress as the viscosity $\mu(\dot{\gamma})$ times the shear rate and integrating over the volume of the channel renders

$$P = \int \mu(\dot{\gamma}) \dot{\gamma}^2 dV \quad (2)$$

Equipped with the previous equation, we can obtain estimates for the power absorbed in the channels of the different spinneret types by COMSOL simulation.

Tensile properties and birefringence

The tensile properties (tenacity (cN/tex); elongation at break (%)) and linear density (dtex)) of the spun fiber samples were measured both in conditioned and wet state using a Favigraph device (Textechno, Germany). Prior to measurement, the fibers were conditioned in 20 ± 2 °C and relative humidity of $65 \pm 2\%$. For each measurement, a total of 20 individual fibers were measured using 20 cN load cell and 20 mm gauge length. The modulus of toughness was calculated using the initial slope of the individual stress strain curves.

The total orientation of the fibers was measured using a polarized light microscope (Zeiss Axio Scope) connected with a 5λ . Berek compensator. The birefringence Δn was calculated from the retardation of the polarized light divided by the thickness of the fiber assuming cellulose density of 1.5 g/cm³ (Männer et al. 2009). The total orientation was calculated from birefringence Δn divided by the maximum value (0.062) of the cellulose's birefringence (Adusumalli et al. 2009; Lenz et al. 1994).

Wide angle X-ray Scattering (WAXS)

X-ray diffraction data of the precursor fibers were collected in the transmission setting of a SmartLab

instrument (RIGAKU) operated at 45 kV and 200 mA. Cellulose fibers were grinded using a Wiley mill with 60 μm mesh size. The samples were then pressed into disks using a pellet press instrument with constant force for 30 s. Powder diffraction data were collected from 5° to 60° 2θ by $\theta/2\theta$ setting. Scattering profile were corrected for smoothing, subtracting air scattering, and subtracting inelastic contribution. Guizani et al. presented the detailed smoothing procedure which was used to subtract the amorphous cellulose contribution from remained elastic scattering profile (Guizani et al. 2020a). Thus, estimated amorphous contribution ($I_{bkg}(2\theta)$) is used to estimate the crystallinity index (CI) using a range from 9° to 50° 2θ :

$$CI = 100 * \frac{\int I(2\theta) d2\theta - \int I_{bkg}(2\theta) d2\theta}{\int I(2\theta) d2\theta} \quad (3)$$

The background corrected profiles were fitted with four pseudo-Voigt functions for (1 $\bar{1}$ 0), (110), (020), and (002) peaks for cellulose II (Langan et al. 2001) using a LMFIT software (Newville et al. 2016). The (002) peak was added because there was a visible shoulder for the peak in this $\theta/2\theta$ and transmission geometry. The Scherrer equation was used to estimate the crystal widths (CW_{hkl}) as follows:

$$CW_{hkl} = \frac{K\lambda}{\beta_{hkl} \cos \theta} \quad (4)$$

where $K = 0.90$ is the shape factor, λ is the X-ray wavelength, β_{hkl} is the full width at half maximum (FWHM) of the diffraction peak in radians, and θ is the diffraction angle of the peak. Due to the significant overlap of (110) and (020) peaks, the crystal widths were reported as average values.

The orientation distribution between fiber axis and the crystallographic (020) lattice plane ($\cos^2 \varphi_{020}$) was estimated using azimuthal scans obtained from the (020) lattice plane of cellulose II allomorph at 21.9° 2θ .

$$\cos^2 \varphi_{020} = \frac{\int_0^{\pi/2} I(\varphi_{020}) \sin \varphi_{020} \cos^2 \varphi_{020} d\varphi}{\int_0^{\pi/2} I(\varphi_{020}) \sin \varphi_{020} d\varphi} \quad (5)$$

The orientation distribution from equatorial diffraction further converted to the orientation distribution between fiber and crystallographic c-axis $\cos^2 \varphi_c$ assuming cylindrical symmetry:

$$\cos^2 \varphi_c = 1 - 2 \cos^2 \varphi_{020} \quad (6)$$

Hermans orientation parameter (f_{WAXD}) was estimated by:

$$f_{WAXD} = \frac{3 \cos^2 \varphi_c - 1}{2}. \quad (7)$$

Small angle X-ray Scattering (SAXS)

SAXS experiment was performed in a transmission mode of Xeuss 3.0 (Xenocs) CuK α X-ray instrument operated at 50 kV and 0.6 mA. Fiber samples were placed vertically on the sample holder and X-ray was radiated on the longitudinal side of the fiber. The sample chamber was kept under vacuum condition (= 0.16 mbar) during the measurement. The scattering intensity was recorded on a 2D detector Eiger2 R 1 M (Detris) and later corrected for the cosmic background.

The azimuthal profile was obtained in a scattering vector Q-range of 0.016–0.002 Å⁻¹ with intensity corrected for the detector orientation, acquisition time, and transmitted flux. The data were not corrected for the sample thickness. The obtained azimuthal profiles were fitted with a pseudo-Voigt function with a constant background. The fitted azimuthal profile was used to estimate the orientation distribution of the equatorial streak $\cos^2 \varphi_{streak}$:

$$\cos^2 \varphi_{streak} = \frac{\int_0^{\pi/2} I(\varphi_{streak}) \sin \varphi_{streak} \cos^2 \varphi_{streak} d\varphi}{\int_0^{\pi/2} I(\varphi_{streak}) \sin \varphi_{streak} d\varphi} \quad (8)$$

Then it was converted into the orientation parameter (f_{SAXS}) in the same fashion as the Hermans orientation parameter is estimated from the equatorial diffraction assuming cylindrical symmetry:

$$\cos^2 \varphi_c = 1 - 2 \cos^2 \varphi_{streak} \quad (9)$$

$$f_{SAXS} = \frac{3 \cos^2 \varphi_c - 1}{2} \quad (10)$$

Scanning electron microscopy (SEM) imaging

SEM imaging was performed by using a Zeiss Sigma VP (manufactured country Germany). For cross-section imaging, the fiber was prepared by cryofracture in liquid nitrogen. A bundle of fiber was first

dipped into liquid nitrogen and snapped. The fractured fiber bundle was then glued onto the conductive support. The samples were sputter-coated with gold to ensure electric conductivity (20 mA current with 90 s coating time). The secondary electron images were taken at a 3 kV operating voltage at ~ 5 k to 10 k magnification.

Results and discussion

Rheology of cellulose solutions

The spinning performance is predominantly modulated by the rheological properties of the dope (Asaadi et al. 2018). The rheology properties of a cellulose solution influence the spinnability of the spinning solution. According to previous studies, cellulose solution in [DBNH][OAc] followed the optimum characteristics of a spinnable solution having zero shear viscosity (20,000–30,000 Pa.s), crossover point around 4000 Pa, and angular frequency around 1 s⁻¹ (Sixta et al. 2015; Hummel et al. 2016; Michud et al. 2015). In this study, for STG cellulose solutions, the average spinning temperature was 72 ± 6 °C, in which the cellulose solutions had average zero shear viscosity ~ 34,000 Pa; complex viscosity at the crossover point, $G' = G''$, ~ 3900 Pa and the angular frequency, $\omega \sim 0.7$ s⁻¹ (Fig. 1). In addition, the denser hole containing spinneret (504 holes) reduced spinning temperature slightly compared to 216-hole spinneret (Table S2). With the increasing number of holes, the mass flow increases resulting in pressure reduction. To maintain the extrusion pressure, the temperature needs to be reduced slightly. Additionally, since the cooling in the air gap is lower with a high number of holes and hole density, the temperature of the supplied spinning solution can be reduced.

Due to having a higher degree of polymerization (DP) and higher molecular weight of HPG pulp, the rheological properties of HPG cellulose solution (13 wt%) are changed significantly compared to the STG cellulose solution (Fig. 1). Interestingly, on average, the spinning temperature for HPG solution was increased by only ~ 6 °C (from 72 to 78 °C) although the HPG solution's zero shear viscosity was higher at the spinning temperature by a factor of 1.9 compared to the STG solution (Fig. 1).

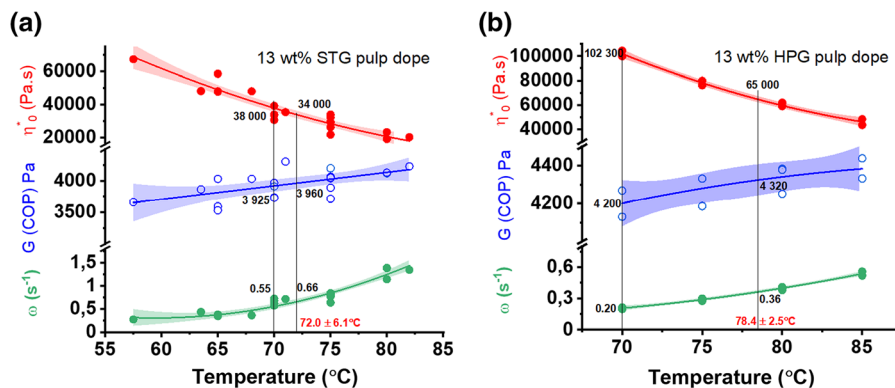


Fig. 1 The rheological parameters including zero shear viscosity η_0^* , dynamic modulus at crossover point; G(COP) and angular frequency at crossover point; ω (COP); of **a** 13 wt%

STG and **b** 13 wt% HPG cellulose solutions in [DBNH][OAc] as a function of temperature. Polynomial fit, 95% confidence band (Origin software)

To observe the effect of the different spinneret geometries, initial spinning trials using different spinneret geometries were performed with STG cellulose solutions with 13 wt% concentration. Later, the HPG cellulose solution was used in combination with optimized spinneret geometry to observe the effect of pulp.

Numerical simulations using cellulose (STG pulp) solution in ionic liquid [DBNH][OAc]

Numerical simulations were performed initially for STG cellulose solution (based on the rheology) inside the spinneret to observe the effect of spinneret geometries in the flow behavior of the cellulose solution. The impact of the shear flow was estimated by integrating the product of the shear velocity and the shear rate over the different capillaries (Fig. 2a,b). According to Xia et al. spinneret aspect ratio and entrance angle determined the IL/cellulose solution flow (Xia et al. 2014, 2015). In this study, the entrance angle of the spinneret influenced the shear power of the STG cellulose dopes inside the spinneret (Fig. S2). The shear power increased significantly due to a lower entrance angle of 8° (rectangular hole distribution) compared to an entrance angle of 60° (circular hole distribution). Previous studies suggested that a shorter entrance angle can be useful to promote efficient solution flow inside the spinneret (Xia et al. 2014). In another study, it was explained that the lower entrance angle reduced the velocity gradient along the flow direction resulting in the extension of the flow length,

which provides the polymer chains enough time to relax (Xia et al. 2016).

The variation of the diameter of the exit channel significantly influences the velocity, pressure, and the shear rate fields in the spinneret. At constant mass flow, variation of the diameter results in different extrusion velocities that affects the shear rate in the spinneret. The deformation energy might be more dissipated in the spinneret with a smaller diameter compared to the wider diameter (Xia et al. 2016). For the spinneret with entrance angle 8°, the diameters were varied from 100, 80, and 50 μm . Earlier studies explained that reduction of the spinneret's hole diameter promoted efficient cooling of the fluid filament in the airgap due to the increased surface area of the filament (Michud et al. 2016; Mortimer and Peguy 1996). Due to the smaller hole diameter, a shorter draw ratio was sufficient to achieve the desired titer. However, the use of 50 μm diameter spinnerets was not successful. During the spinning the piston pressure inside the spinneret exceeded the optimum pressure at a higher draw ratio which causes fiber breakages. The use of this D50 spinneret may require a lower cellulose concentration in the dope for successful spinning (less than 13 wt%). Hence, the numeric simulations of the cellulose solutions' flow behavior inside the D50 spinneret were not performed. The viscous power (shear power) of the STG cellulose solution into both D100 and D80 spinnerets varied with the change in capillary length. In case of D100 spinnerets, the spinneret capillary aspect ratio increased from L/D 0.2 to L/D 1.0, 1.5, 2, 4, and 5. The shear power increased by a factor of 1.15 when the

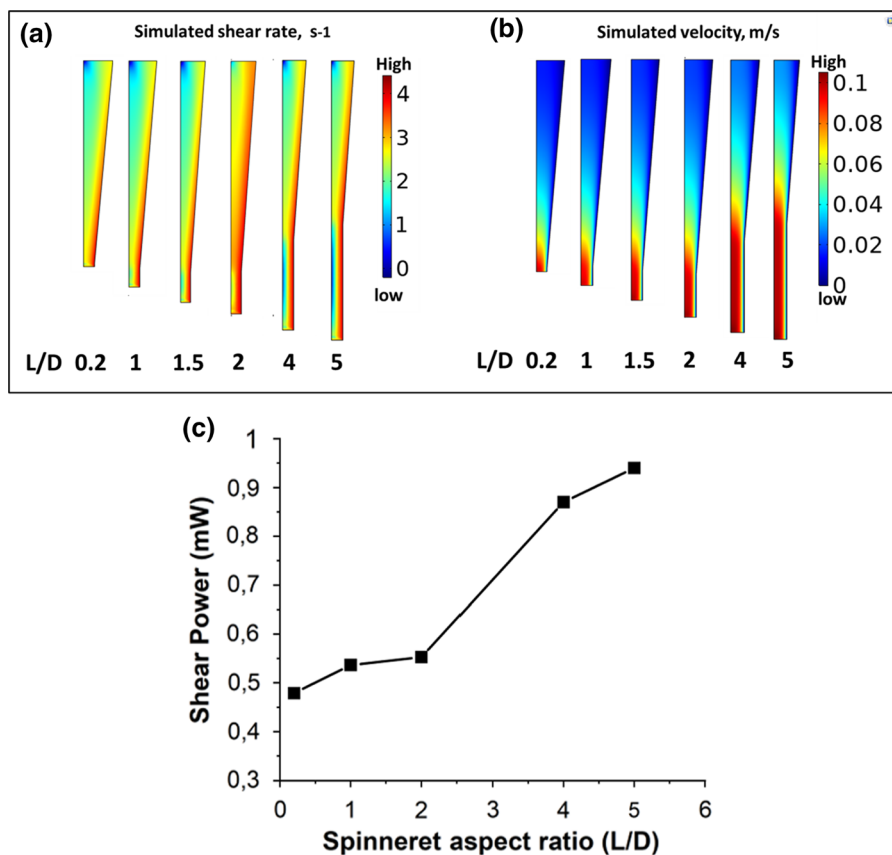


Fig. 2 **a** Logarithm of the simulated shear rate (left) and **b** simulated velocities for the D100 spinnerets (L/D 0.2, 1, 1.5, 2, 4, 5); **c** Simulated shear power with increasing capillary lengths

of the spinnerets with 100 μm diameter for the 13 wt% STG cellulose solutions in [DBNH][OAc]

capillary aspect ratio was increased from L/D 0.2 to 1.0–2.0, while when increased to L/D 4 and 5, the shear powers increased by a factor of 1.8 to 1.9, respectively (Fig. 2c). On the other hand, for D80 spinnerets, the shear power increased slightly for the enhanced capillary length (L/D 0.2 to 1.0) (Fig. S3).

Investigation of the effect of spinneret geometries on the mechanical properties of fibers

Spinneret geometries: titer (linear densities) and spinnabilities

The spinnability of a cellulose solution is defined by the stretchability of a fluid filament in the airgap for a defined time without breakage. This filament stretchability is characterized by the ratio of take-up velocity to extrusion velocity named as draw ratio (DR). The linear density (titer) of the spun fibers are adjusted by

the DR (Hauru et al. 2014). In several previous research studies, the spinnability of a cellulose solution spun with 100 μm hole diameter spinnerets was defined as follows: DR < 2 (titer > 6 dtex); non-spinnable, DR 2–8 (titer 6–2 dtex) -poor, DR 8–14 (titer 2–1 dtex) -good and DR > 14 (titer < 1 dtex) -excellent (Asaadi et al. 2016, 2018; Haslinger et al. 2019a).

Compared to D100 spinnerets, the fibers with target titer were produced at a lower DR using D80 spinnerets (Fig. 3a,b). The decrease in spinneret diameter reduces the draw length (Mortimer and Péguy 1995). Based on the titer measurement, the spinnability can be defined as follows using a spinneret with a hole diameter of 80 μm : DR < 5 (titer > 2) -poor, DR 5–9 (2–1 dtex) -good and DR > 9 (titer < 1 dtex) -excellent. In addition, the spinnability was determined in terms of the minimum titer achieved and considering the spinning time of

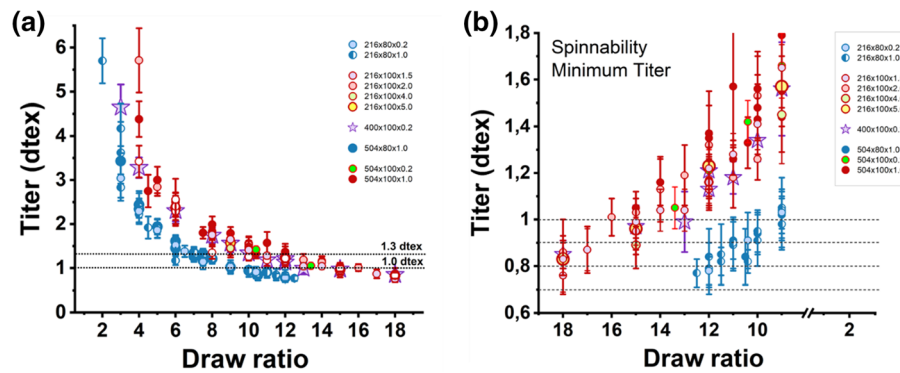


Fig. 3 The titer (linear density) and draw ratio (DR) relationship of the fibers spun from different spinneret geometries **a** titer 0.5–6 dtex **b** titer 0.6–1.8 vs DR 2–18. Pulp & solvent: 13 wt% STG cellulose concentration in [DBNH][OAc]

5 min throughout at this DR. The spinnabilities of the use of different spinnerets are listed in Table S1. In this study, all the spinnerets with hole diameter 100 μm and 80 μm showed good to excellent spinnabilities for both STG and HPG cellulose solutions regardless of the spinneret aspect ratio.

L/D ratio of the spinnerets: effect on toughness and tenacity

According to our previous study, the longer capillary ($D = 100$; $L = 200$; $L/D = 2$) influenced the molecular alignment of the cellulose molecule of a cellulose solution with high shear power inside the spinneret (Moriam et al. 2021b). It was reported that, the high shear flow inside the longer capillary spinneret reduced the entanglement of the polymer chains and at the same time promoted effective molecular alignment along the flow direction. As a result, fiber toughness improved considerably. Hence, the target of this study was to further study the effect of the spinneret length-to-diameter ratio (L/D) in the fiber mechanical properties, particularly in the fiber toughness when the L/D was extended up to 5.

Interestingly, maximum tenacity and toughness were achieved at titers ranging from 1.0 to 1.2 dtex regardless of the spinneret geometry (Fig. 4a,b). Additionally, the highest toughness and tenacities of the fibers were achieved for the spinnerets having $L/D = 1.0$ – 2.0 . Longer capillary of $L/D = 4$ and 5 did not improve the fiber toughness. Due to the high shear power within the longer capillaries of $L/D = 4$ and 5 , the shear stress presumably becomes so high above a certain DR that partial cohesive fractures are likely to

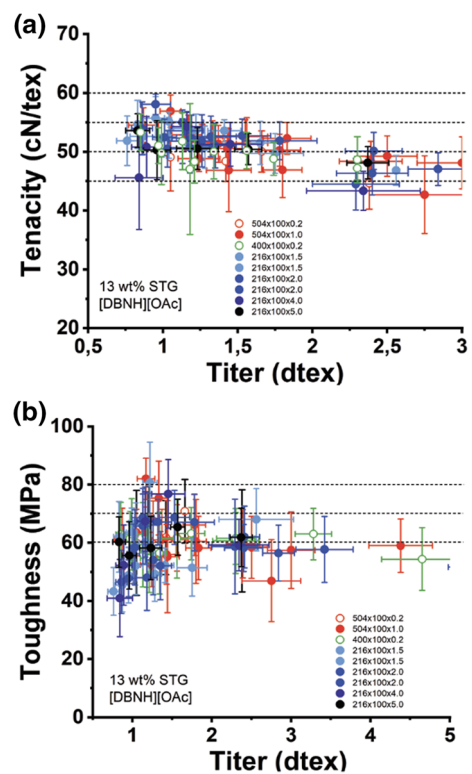


Fig. 4 The achieved **a** tenacities and **b** toughness of the fibers at different titers spun from D100 spinnerets with different length-diameter ratios ($L/D = 1, 1.5, 2, 4, \text{ and } 5$). Pulp & solvent: 13 wt% STG cellulose concentration in [DBNH][OAc]

occur, reflecting a stagnant or even decreasing toughness modulus with increasing DR. As a result, the fiber toughness decreased sharply at titers around 0.8 dtex (Fig. 4a).

The contour plots further confirmed that high tenacity and toughness of the fibers were produced

using the spinnerets with L/D ratio of 1–2 (Fig. S5a and S5b). As previously discussed, the numeric simulations showed that the shear power increased by a factor of 1.15 when L/D increased from 0.2 to 1.0–2.0. On the other hand, the shear power for L/D 4 and 5 was enhanced by a factor of 1.8 and 1.9, respectively. An optimum increase of shear power, rather than too high shear power of the solution flow inside spinneret, might be favorable for better mechanical properties of the fiber. Lundahl et al. reported in a review study a similar observation where the dry-spun CNF filaments showed maximum strength at an optimum spinning shear beyond which the mechanical properties of the CNF filament started to decrease (Lundahl et al. 2017). Another study showed that with the increased shear rate during wet spinning of polyethersulfone hollow fiber, the tensile strength and young modulus of the fiber increased but elongation at break decreased. They explained that the high shear rate promoted greater orientation and more closely packed molecular chains in the direction of shear which substantially increased the tensile strength at break but introduced higher resistance to elongation at break (Chung et al. 2000). In this study, with an increased capillary ratio of more than L/D 2 at target titer, the tensile strength did not change significantly, but the elongation at break decreased (Table S3). High shear power induced by a longer capillary ($L/D > 2$) might create irreversible molecular chain arrangement and restrict the elongation. Thus, the tensile strength and the young's modulus remained unchanged, but the elongation at break decreased, resulting in a slight reduction in fiber toughness. The reduction in elongation and toughness of the fiber was more prominent at the target titer (~ 1.2 – 1.3 dtex) while using spinneret with L/D 5 (Fig. 4b, Table S3).

Furthermore, the microfibers with a titer below 1.0 dtex showed a significant reduction in toughness, especially for longer capillaries ($L/D > 2$) (Fig. 4b and Fig. S5). As the titer decreases, the elastic stress increases once all the chains reach their maximum elongated state (Bengtsson et al. 2021). At some point, the filaments get too thin that the shear stress exceeds the tensile strength of the filament leading to a gradually increasing cohesive fracture (Fisher and Denn 1976). The resulting lower lateral intercrystallite interaction causes a reduced elongation of the fibers produced (Schurz and Lenz 1994). At the same time,

the modulus of elasticity increases with decreasing titer to a point where fiber breakages started during spinning (Fig. S8).

Hole diameter of the spinnerets: effect on toughness and tenacity

Since the highest toughness and tenacities of the fibers were obtained when using D100 spinnerets with L/D 1–2, the highest aspect ratio of L/D 1 was selected for D80 spinnerets. In the case of the D80 spinneret, the effect of different spinneret capillary aspect ratios was compared between L/D 1 (longer) and L/D 0.2 (shorter). Similar to D100, the shear power of the cellulose solution inside the D80 with the spinneret of a larger L/D ratio was slightly higher than that of shorter capillary L/D 0.2 (Fig. S3). Interestingly, the tenacity and toughness of the spun fibers at target titer (1–1.3 dtex) produced using D80 was almost similar

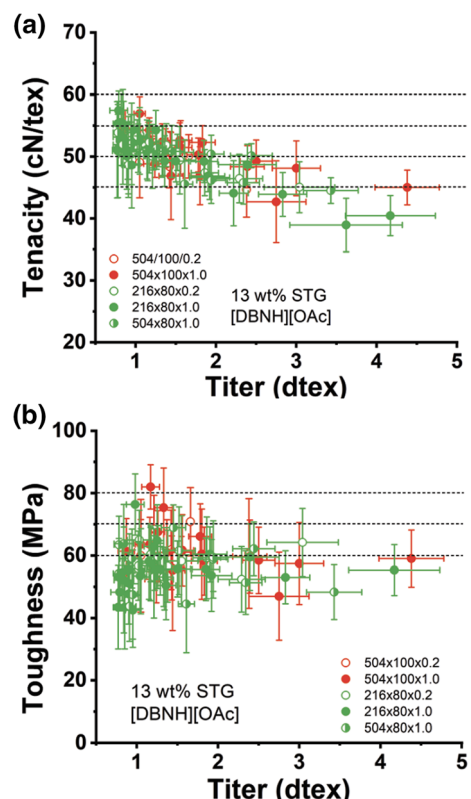


Fig. 5 The effect of different hole diameters (80 and 100 μm) and the capillary diameter to length ratio, L/D (short; L/D 0.2 and long capillary; L/D 1.0) on **a** tenacities and **b** toughness of the spun fibers at different titers. Pulp & solvent: 13 wt% STG cellulose concentration in [DBNH][OAc]

for both shorter and longer capillaries (Fig. 5a,b; Table S3). The optimum shear power might already be achieved with a reduction of the diameter from 100 to 80 μm , so that a further increase of the capillary aspect ratio had no influence on the mechanical properties of the fibers spun with D80. The use of D100 and D80 spinnerets showed comparable results (Fig. 5a,b; Fig. S6).

In terms of fiber toughness improvements, the 504-hole spinneret showed slight advantages over the 216-hole spinneret (Fig. 5a,b). As mentioned earlier, the required spinning temperature was lower when spinning with spinnerets with a larger number of orifices. The lower temperature of the solution means a higher solution viscosity, which is associated with a relatively higher elongational viscosity (Guizani et al. 2020b). This high elongational viscosity could contribute to the improvement of tenacity and toughness of the spun fibers.

Assessing the effect of spinneret geometries in combination with different pulp properties

Effect of pulp purity: 100 and 80 μm diameters

STG fibers with highest toughness and tenacity were produced using a spinneret with L/D 1. Hence, the effect of pulp purity in the final fiber was investigated using two different spinnerets with L/D 1 (longer capillary) and L/D 0.2 (shorter capillary).

A longer capillary (L/D 1.0) was clearly advantageous compared to the shorter capillary (L/D 0.2) for achieving both high tenacity and high toughness (Fig. 6a and b). In addition, HPG with longer and more uniform molecular chains (lower polydispersity) in combination with high viscosity resulted in improved mechanical properties. A previous study indicated that a higher proportion of longer molecular chains, lower polydispersity, and fewer non-cellulosic impurities in an HPG pulp resulted in improved mechanical properties of fibers spun from it compared to fibers spun from an STG pulp (Moriyam et al. 2021b). Fibers spun from HPG-IL solution with a longer capillary (L/D 1.0) further improved toughness compared to fibers spun from HPG in combination with a shorter capillary (L/D 0.2) (Fig. 6b). In combination with a longer capillary (L/D 1) and high-purity pulp, the maximum fiber toughness reached up to 93 MPa at a titer of ~ 1.3 dtex (Fig. 6b,

Table S3), which can be considered the best mechanical properties achieved so far for Ioncell fibers.

In terms of both tenacity and toughness of fibers produced with D100 spinnerets, the effects caused by the combination of HPG and short capillary (L/D 0.2) and those produced by STG and longer capillary (L/D 1) were comparable (Fig. 6a,b).

In case of D80 spinnerets, fiber produced from HPG pulp also showed better mechanical strength compared to fibers spun from STG (Fig. 6c,d). However, the difference was not as prominent as it was for the fibers produced from D100 spinnerets. This might be related to the changed shear flow behavior inside the spinneret. The numerical simulation showed that when the D100 spinneret was used, the shear power increased for both longer capillaries (L/D 1) and presence of HPG dopes in the capillaries (Fig. S4). However, the two different cellulose solutions (13 wt%) prepared from STG and HPG pulps, respectively, showed no difference in shear power when the D80 spinneret was used (Fig. S4).

Pulp concentration: effect on toughness and tenacity

In a previous publication, the cellulose concentration in a [DBNH][OAc] solution was varied from 10 to 17 wt% and it was reported that the mechanical properties of the fiber were highest while using a cellulose concentration of 15 wt% (Sixta et al. 2015). In this study, to investigate the effect of increased cellulose concentration in the spinning solution on fiber properties, cellulose solutions containing 15 wt% cellulose (using both STG and HPG) were prepared and spun in comparison with solutions containing 13 wt% cellulose.

Interestingly, the fiber properties showed no further improvement with increasing concentration, regardless of the change in the pulp (Fig. 7a–d). Rather, both fiber tenacity and toughness decreased compared to the fibers spun from 13 wt% cellulose concentration (Fig. 7a–d). The 15wt% and 17wt% cellulose solutions were previously spun (Sixta et al. 2015) with a circular spinneret in which the capillaries had a larger entrance angle (60°). However, in this study, the spinneret with rectangular hole distribution had a narrower entrance angle of only 8° , the latter exerting a significantly higher shear power on the cellulose solution than a spinneret with a larger entrance angle (Figure S2). Due to the high shear power, the solution

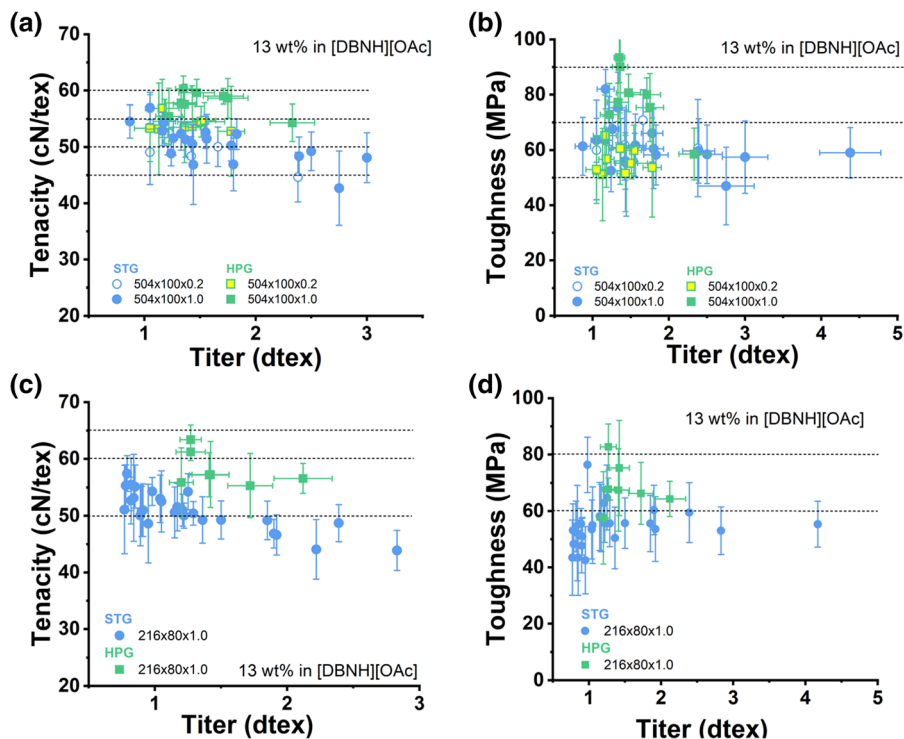


Fig. 6 Effect of STG and HPG pulps in the **a** tenacity and **b** toughness of the fibers produced using 100 μm spinneret with short (L/D 0.2) and long (L/D 1.0) capillary; the effect of STG

and HPG in **c** tenacity and **d** toughness of the fibers produced using 80 μm spinneret having L/D 1.0. Pulp & solvent: STG and HPG (13 wt% cellulose concentration in [DBNH][OAc])

flow might be restricted at high cellulose concentration in the dope so that the shear stress became higher with increasing zero shear viscosity (Table S4), resulting in partial cohesive fracture, which impaired the mechanical properties of the spun fibers.

Structural properties of the high toughness fibers

Both the elongation and tensile strength properties of the fiber depend on the fiber orientation (Asaadi et al. 2018). Hence, toughness, which is the integral of the tensile strength over the elongation, also depends on fiber orientation. Previous studies have shown that the degree of fiber orientation increased considerably at a lower DR and tended to level-off when greater than 5 (Michud et al. 2016). Both the total orientation and crystalline orientations of the fibers were nearly the same for the STG- and HPG-based fibers regardless of the spinneret geometries (Fig. 8). In addition, the change in crystal size and crystallinity did not correlate with the change in toughness of the fiber.

The average crystal size of the fibers was 34–36 Å and the crystallinity was 34–36% (Table S3).

The voids within the fiber matrix influence the mechanical properties of the fiber. In the dry-jet wet spinning process, the microvoids are elongated and formed in the spinneret (pre-orientation) and in the airgap (Schurz et al. 1995; Sharma et al. 2019). Previously, the microvoid orientation of the HPG-based fibers were found to be lower compared to the STG fiber (Moriam et al. 2021b). It was assumed that the slightly reduced microvoid orientation of the HPG-based fiber improved the extensibility of fibers resulting in a concomitant increase in elongation properties along with the increased tensile strength. Consistent with the previous studies, HPG-based fibers produced in this study also showed reduced microvoid orientations compared to the STG-based fibers (Fig. 9). Additionally, gradual reduction in microvoid orientation was observed for the fibers with increased toughness regardless of their origins (Fig. 9).

Lyocell fibers have a skin–core structure, but with a much thinner skin (outer layer) than regular viscose

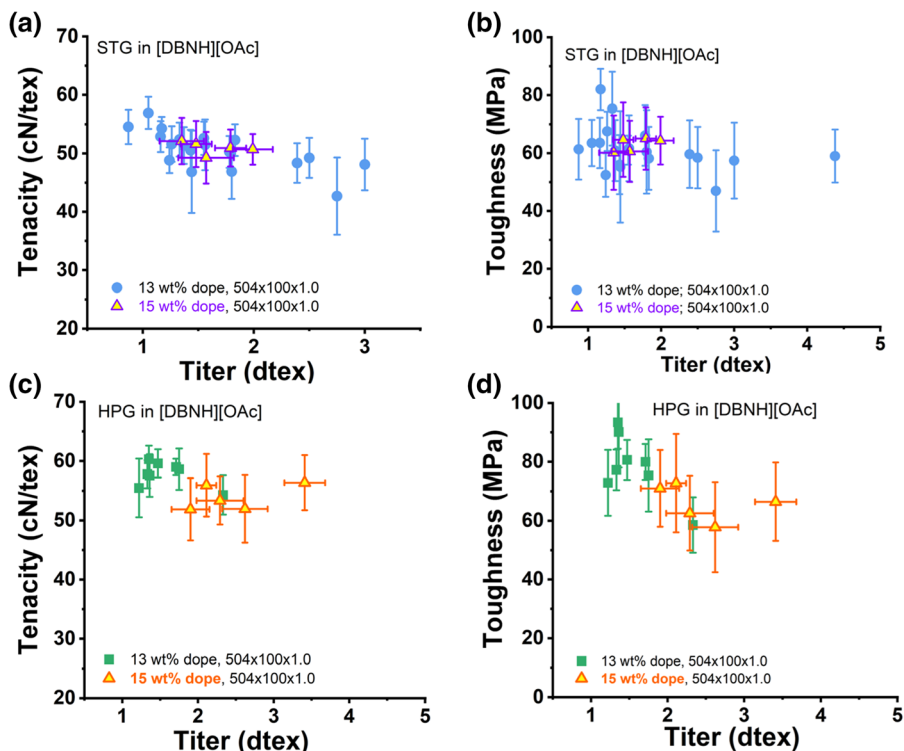


Fig. 7 The effect of increased STG and HPG cellulose concentration (13 wt% to 15 wt% in [DBNH][OAc]) in **a** tenacity and **b** toughness of STG-based fibers; **c** tenacity and **d** toughness of HPG-based fibers

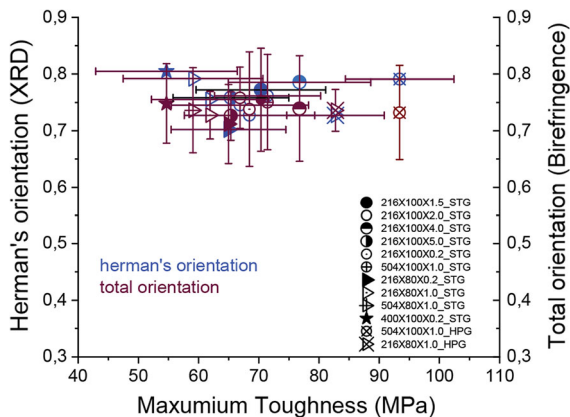


Fig. 8 The total orientation and crystalline orientation values for the high toughness STG- and HPG-based fibers spun using different geometries (in terms of diameters and capillary aspect ratio). Pulp & solvent: STG and HPG (13 wt% cellulose concentration in [DBNH][OAc])

(CV) fibers and an inner crystalline core consisting of nearly parallel oriented fibrils connected to amorphous domains (Biganska and Navard 2008).

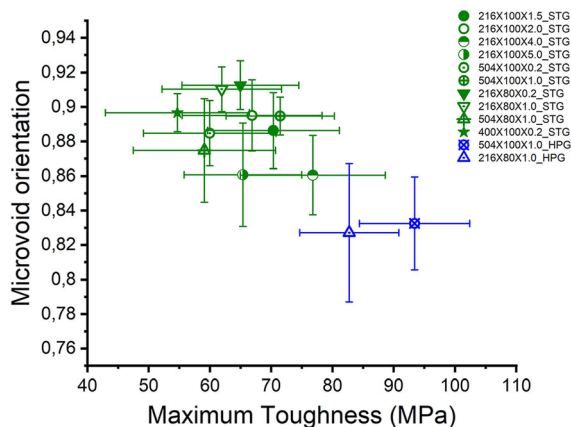


Fig. 9 The microvoid orientation of the STG- and HPG-based fibers with maximum toughness produced using different spinneret geometries. Pulp and solvent: STG and HPG (13 wt% cellulose concentration in [DBNH][OAc])

Fiber morphologies were nearly identical for all fibers prepared from HPG and STG (Fig. 10), regardless of their process parameters such as spinneret geometries and raw materials. Analogous to the lyocell fibers spun from NMMO cellulose spinning

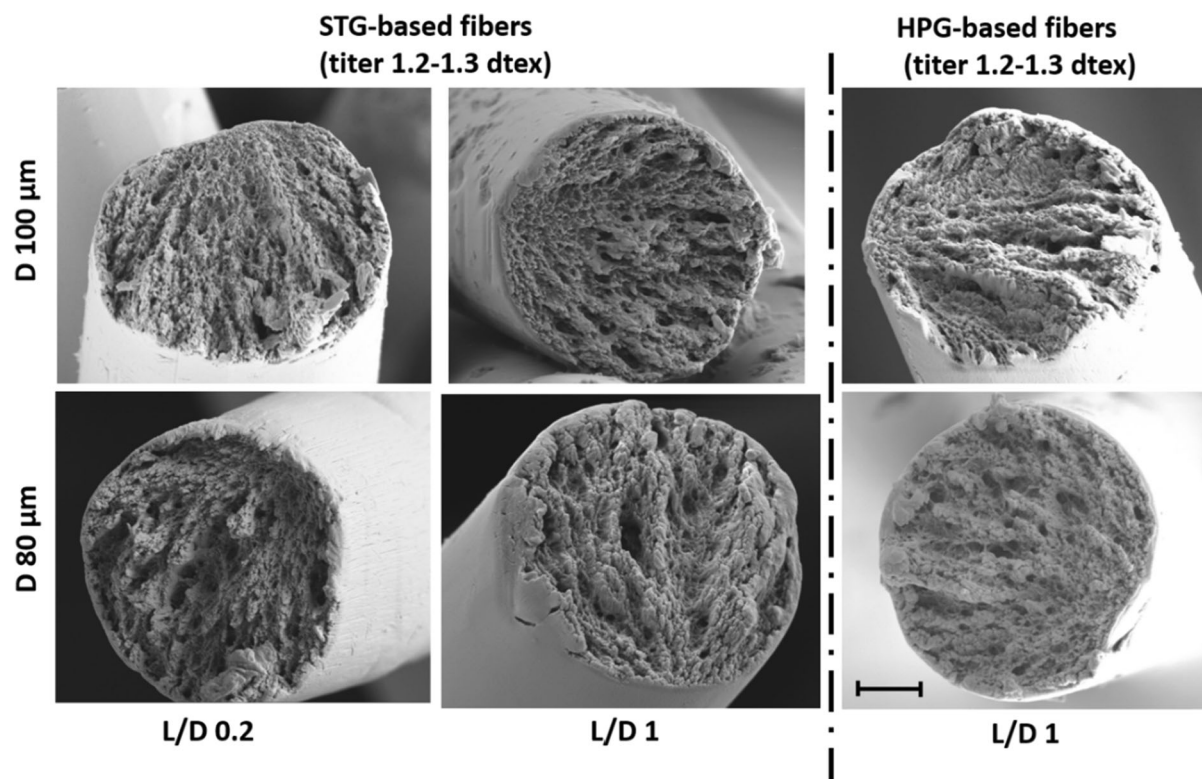


Fig. 10 The morphologies of the spun fibers of standard titer spun using 100 μm and 80 μm spinneret diameters (STG-based fibers: L/D 0.2 and 1.0; HPG-based fibers: L/D 1.0). Scale bar

2 μm . Pulp and solvent: STG and HPG; 13 wt% cellulose concentration in [DBNH][OAc]

solutions, the Ioncell fibers were exhibited a skin–core structure with a thin outer layer and an inner core from which oriented fibrils protruded surrounded by somewhat irregularly arranged voids (open pores).

Qualitatively, the diameters of the microvoids in the fibers spun with the longer capillaries, L/D = 1 and a hole diameter of 100 μm , are larger and less oriented than those of the reference fibers spun with the shorter capillaries, L/D = 0.2. These differences in the fibrillar structure of the fiber cross sections also apply to the microfibers with a titer smaller than 1.0 (Fig. S7).

Conclusion

The development of a circular economy requires strategies to produce cellulosic fibers with high toughness, as fiber toughness is the core for improving the longevity of cellulose-based textiles. Biodegradable and cellulose-based fibers from closed loop operations are the sustainable solution to meet

challenges in the textile industry such as microplastic pollution and non-recyclable textiles. Ioncell technology has already shown tremendous potential for textile recycling and the production of cellulose-based textile fibers with superior strength properties compared to any other cellulose-based fibers on the market. In this study, certain process settings were investigated to enhance fiber toughness, giving priority to the spinneret geometry. The spinneret geometry exhibited a significant effect on the mechanical properties of the fiber spun from the ionic liquid [DBNH][OAc]. Numerical simulations showed that the flow properties of the cellulose solution changed with different spinneret geometries. The spinneret with a capillary aspect ratio L/D 1–2 provided optimized shear power of the cellulose solution, which is required for a better mechanical property of the spun fiber. Spinneret L/D 1–2 promoted the highest tenacity and toughness of the fibers. Both D100 and D80 showed comparable fiber properties. The combination of the use of high-purity pulp (13 wt%) and the capillary aspect ratio L/D

1 with a capillary entry cone 8° of the D100 spinneret resulted in fibers with the highest toughness (93 MPa) and a tenacity of 60 cN/tex. With the new strategies presented in this study, Ioncell fibers were able to achieve approximately 12% higher toughness as compared to the previous study (from 83.3 to 93 MPa) (Moriam et al. 2021b). Both total and the crystalline orientation showed no significant changes for the high-toughness fibers spun from different geometries or raw materials. The microvoid orientations were comparatively lower for the HPG-based fibers than for the STG-based fibers, while the fiber morphologies for the spun fibers were very similar at a standard titer, but still showed qualitatively larger pore structures for the HPG fibers.

Finally, this research created a new perspective for improving the toughness of cellulose-based textile fiber which will contribute to the circular economy and sustainability of textile production. Further studies will include the effect of different spinneret geometries at even larger variations on the mechanical properties of Ioncell fibers made from other ionic liquids.

Acknowledgments This project has received funding from the Academy of Finland (under the project WTF-click-nano), Jenny and Antti Wihuri foundation, Puunjalostusinsinöörit Oy and FinnCERES. The authors also gratefully acknowledge Katrina Rätty for proofreading the article. Additionally, the authors acknowledge the provision of facilities and technical support by Aalto University at OtaNano -Nanomicroscopy Center (Aalto-NMC) and D22 instrument at ILL, Dr. Lionel Porcar.

Author contributions Herbert Sixta and Kaniz Moriam designed and interpreted the results of all the experiments. The manuscript was written by Kaniz Moriam as a principal author and Herbert Sixta reviewed the manuscript. All authors have given approval to the final version of the manuscript.

Funding Open access funding provided by Aalto University.

Declarations

Conflict of interest The authors declare that they have no conflict of interest.

Human and animal rights This research does not contain any experiments with human participants or animals.

Open Access This article is licensed under a Creative Commons Attribution 4.0 International License, which permits use, sharing, adaptation, distribution and reproduction in any medium or format, as long as you give appropriate credit to the

original author(s) and the source, provide a link to the Creative Commons licence, and indicate if changes were made. The images or other third party material in this article are included in the article's Creative Commons licence, unless indicated otherwise in a credit line to the material. If material is not included in the article's Creative Commons licence and your intended use is not permitted by statutory regulation or exceeds the permitted use, you will need to obtain permission directly from the copyright holder. To view a copy of this licence, visit <http://creativecommons.org/licenses/by/4.0/>.

References

- Adusumalli RB, Keckes J, Martinschitz KJ, Boesecke P, Weber H, Roeder T, Gindl W (2009) Comparison of molecular orientation and mechanical properties of lyocell fibre tow and staple fibres. *Cellulose* 16:765–772. <https://doi.org/10.1007/s10570-009-9292-2>
- Asaadi S, Hummel M, Ahvenainen P, Gubitosi M, Olsson U, Sixta H (2018) Structural analysis of Ioncell-F fibres from birch wood. *Carbohydr Polym* 181:893–990. <https://doi.org/10.1021/acssuschemeng.8b01768>
- Asaadi S, Hummel M, Hellsten S, Härkäsalmi T, Ma Y, Michud A, Sixta H (2016) Renewable high performance fibers from the chemical recycling of cotton waste utilizing an ionic liquid. *Chemoschem* 9:3250–3258. <https://doi.org/10.1002/cssc.201600680>
- Bengtsson J, Jedvert K, Köhnke T, Theliander H (2021) The challenge of predicting spinnability: investigating benefits of adding lignin to cellulose solutions in air-gap spinning. *J Appl Polym Sci* 138:50629. <https://doi.org/10.1002/app.50629>
- Biganska O, Navard P (2008) Morphology of cellulose objects regenerated from cellulose–N-methylmorpholine N-oxide–water solutions. *Cellulose* 16(2):179. <https://doi.org/10.1007/s10570-008-9256-y>
- Chung TS, Qin JJ, Gu J (2000) Effect of shear rate within the spinneret on morphology, separation performance and mechanical properties of ultrafiltration polyethersulfone hollow fiber membranes. *Chem Eng Sci* 55(6):1077–1091. [https://doi.org/10.1016/S0009-2509\(99\)00371-1](https://doi.org/10.1016/S0009-2509(99)00371-1)
- Fisher RJ, Denn MM (1976) A theory of isothermal melt spinning and draw resonance. *AIChE J* 22:236–246. <https://doi.org/10.1002/aic.690220203>
- Elsayed S, Hellsten S, Guizani C, Witos J, Rissanen M, Rantamäki AH, Varis P, Wiedmer SK, Sixta H (2020) Recycling of superbase-based ionic liquid solvents for the production of textile-grade regenerated cellulose Fibers in the Lyocell process. *ACS Sustain Chem Eng* 8:14217–14227. <https://doi.org/10.1021/acssuschemeng.0c05330>
- Guizani C, Larkiala S, Moriam K, Sawada D, Elsayed S, Rantasalo S, Hummel HM (2020) Air gap spinning of a cellulose solution in [DBNH][OAc] ionic liquid with a novel vertically arranged spinning bath to simulate a closed loop operation in the Ioncell® process. *J Appl Polym Sci* 138(5):49787. <https://doi.org/10.1002/app.49787>

- Guizani C, Nieminen K, Rissanen M, Larkiala S, Hummel M, Sixta H (2020b) New insights into the air gap conditioning effects during the dry-jet wet spinning of an ionic liquid-cellulose solution. *Cellulose* 27(9):4931–4948. <https://doi.org/10.1007/s10570-020-03115-8>
- Haslinger S, Hummel M, Anghelescu-Hakala A, Määttänen M, Sixta H (2019a) Upcycling of cotton polyester blended textile waste to new man-made cellulose fibers. *Waste Manage* 97:88–96. <https://doi.org/10.1016/j.wasman.2019.07.040>
- Haslinger S, Wang Y, Rissanen M, Lossa MB, Tanttu M, Ilen E, Määttänen M, Harlin A, Hummel M, Sixta H (2019b) Recycling of vat and reactive dyed textile waste to new colored man-made cellulose fibers. *Green Chem* 21(20):5598–5610. <https://doi.org/10.1039/C9GC02776A>
- Hauru LKJ, Hummel M, Michud A, Sixta H (2014) Dry jet-wet spinning of strong cellulose filaments from ionic liquid solution. *Cellulose* 21(6):4471–4481. <https://doi.org/10.1007/s10570-014-0414-0>
- Hummel M, Michud A, Tanttu M, Asaadi S, Ma Y, Hauru LKJ, Parviainen A, King AWT, Kilpeläinen I, Sixta H (2016) Ionic liquids for the production of man-made cellulosic fibers: opportunities and challenges. In: Rojas OJ (ed) *Cellulose chemistry and properties: fibers, nanocelluloses and advanced materials*. Springer International Publishing, Cham, pp 133–168
- Jiang X, Bai Y, Chen X, Liu W (2020) A review on raw materials, commercial production and properties of lyocell fiber. *J Bioresour Bioproducts* 5:16–25. <https://doi.org/10.1016/j.jobab.2020.03.002>
- Kirichenko A, Kholosha V, Chernyshov YA, Il'in V, Nefedova I, Ambainis YYJFC (1977) The spinneret design as a factor in the conditions of cooling and regularity of the properties of Capron cord yarn. *Fibre Chem* 8(6):642–644. <https://doi.org/10.1007/BF00546688>
- Langan P, Nishiyama Y, Chanzy H (2001) X-ray structure of mercerized cellulose II at 1 Å resolution. *Biomacromol* 2(2):410–416. <https://doi.org/10.1021/bm005612q>
- Lenz J, Schurz J, Wrentschur E (1994) On the elongation mechanism of regenerated cellulose fibres. *Holzforschung* 48(s1):72–76. <https://doi.org/10.1515/hfsg.1994.48.s1.72>
- Lundahl MJ, Klar V, Wang L, Ago M, Rojas OJ (2017) Spinning of cellulose nanofibrils into filaments: a review. *Ind Eng Chem Res* 56(1):8–19. <https://doi.org/10.1021/acs.iecr.6b04010>
- Ma Y, Hummel M, Kontro I, Sixta H (2018a) High performance man-made cellulosic fibres from recycled newsprint. *Green Chem* 20(1):160–169. <https://doi.org/10.1039/C7GC02896B>
- Ma Y, Stubb J, Kontro I, Nieminen K, Hummel M, Sixta H (2018b) Filament spinning of unbleached birch kraft pulps: effect of pulping intensity on the processability and the fiber properties. *Carbohydr Polym* 179:145–151. <https://doi.org/10.1016/j.carbpol.2017.09.07>
- Michud A, Hummel M, Sixta H (2016) Influence of process parameters on the structure formation of man-made cellulosic fibers from ionic liquid solution. *J Appl Polym Sci* 133(30):43718. <https://doi.org/10.1002/app.43718>
- Michud A, Tanttu M, Asaadi S, Ma Y, Netti E, Kääriäinen P, Persson A, Bernström A, Hummel M, Sixta H (2015) Ioncell-F: ionic liquid-based cellulosic textile fibers as an alternative to viscose and Lyocell. *Text Res J* 86(5):543–552. <https://doi.org/10.1177/0040517515591774>
- Moriama K, Rissanen M, Sawada D, Altgen M, Johansson L-S, Evtuyugin DV, Guizani C, Hummel M, Sixta H (2021a) Hydrophobization of the man-made cellulosic fibers by incorporating plant-derived hydrophobic compounds. *ACS Sustain Chem Eng* 9:4915–4925. <https://doi.org/10.1021/acssuschemeng.1c00695>
- Moriama K, Sawada D, Nieminen K, Hummel M, Ma Y, Rissanen M, Sixta H (2021b) Towards regenerated cellulose fibers with high toughness. *Cellulose*. <https://doi.org/10.1007/s10570-021-04134-9>
- Mortimer SA, Péguy A (1995) 72-Spinning of fibres through the N-methylmorpholine-N-oxide process. In: Kennedy JF, Phillips GO, Williams PA (eds) *Cellulose and cellulose derivatives*. Woodhead Publishing, London, pp 561–567. <https://doi.org/10.1533/9781845698539.6.561>
- Mortimer SA, Peguy AA (1996) The influence of air-gap conditions on the structure formation of lyocell fibers. *J Appl Polym Sci* 60(10):1747–1756. [https://doi.org/10.1002/\(SICI\)1097-4628\(19960606\)60:10%3c1747::AID-APP28%3e3.0.CO;2-#](https://doi.org/10.1002/(SICI)1097-4628(19960606)60:10%3c1747::AID-APP28%3e3.0.CO;2-#)
- Männer J, Ivanoff D, Morley RJ, Lenzing SJ (2009) Tencel®-New cellulose fibers for carpets. *Lenzinger Berichte* 2:60–71
- Newville M, Stensitzki T, Allen DB, Rawlik M, Ingargiola A, Nelson AJASCL (2016) Lmfit: non-linear least-square minimization and curve-fitting for python. *Science* 1606:14
- Royer SJ, Wiggin K, Kogler M, Deheynd DD (2021) Degradation of synthetic and wood-based cellulose fabrics in the marine environment: comparative assessment of field, aquarium, and bioreactor experiments. *Sci Total Environ* 791:148060. <https://doi.org/10.1016/j.scitotenv.2021.148060>
- Salvador CF, Turra A, Baruaque-Ramos J (2017) Synthetic fibers as microplastics in the marine environment: a review from textile perspective with a focus on domestic washings. *Sci Total Environ* 598:1116–1129. <https://doi.org/10.1016/j.scitotenv.2017.04.172>
- Sayyed AJ, Deshmukh NA, Pinjari DV (2019a) A critical review of manufacturing processes used in regenerated cellulosic fibres: viscose, cellulose acetate, cuprammonium, LiCl/DMAc, ionic liquids, and NMMO based lyocell. *Cellulose* 26:2913–2940. <https://doi.org/10.1007/s10570-019-02318-y>
- Sayyed AJ, Mohite LV, Deshmukh NA, Pinjari DV (2019b) Structural characterization of cellulose pulp in aqueous NMMO solution under the process conditions of lyocell slurry. *Carbohydr Polym* 206:220–228. <https://doi.org/10.1016/j.carbpol.2018.11.004>
- Schurz J, Lenz J (1994) Investigations on the structure of regenerated cellulose fibers. *Macromol Symp* 83:273–89
- Schurz J, Lenz J, Wrentschur E (1995) Inner surface and void system of regenerated cellulose fibers. *Die Angewandte Makromolekulare Chemie* 229(1):175–184. <https://doi.org/10.1002/apmc.1995.052290112>
- Sharma A, Sen D, Thakre S, Kumaraswamy G (2019) Characterizing microvoids in regenerated cellulose fibers obtained from Viscose and Lyocell processes. *Macromolecules*

- 52:3987–3994. <https://doi.org/10.1021/acs.macromol.9b00487>
- Shen L, Worrell E, Patel MK (2010) Environmental impact assessment of man-made cellulose fibres. *Resour Conserv Recycl* 55(2):260–274. <https://doi.org/10.1016/j.resconrec.2010.10.001>
- Sixta H, Michud A, Hauru L, Asaadi S, Ma Y, King AWT, Kilpelainen I, Hummel M (2015) Ioncell-F: a high-strength regenerated cellulose fiber. *Nord Pulp Pap Res J* 30(1):43–57. <https://doi.org/10.3183/npprj-2015-30-01-p043-057>
- Stone C, Windsor FM, Munday M, Durance I (2020) Natural or synthetic—how global trends in textile usage threaten freshwater environments. *Sci Total Environ* 718:134689. <https://doi.org/10.1016/j.scitotenv.2019.134689>
- Wang J, Wang T, Xu J, Yu J, Zhang Y, Wang H (2018) Study on spinnability of polyacrylonitrile solution based on dynamics simulation of dry-jet wet spinning. *J Appl Polym Sci* 135:46377. <https://doi.org/10.1002/app.46377>
- Wedin H, Lopes M, Sixta H, Hummel M (2019) Evaluation of post-consumer cellulosic textile waste for chemical recycling based on cellulose degree of polymerization and molar mass distribution. *Text Res J* 89(23–24):5067–5075. <https://doi.org/10.1177/0040517519848159>
- Xia X, Gong M, Wang C, Wang B, Zhang Y, Wang H (2015) Dynamic modeling of dry-jet wet spinning of cellulose/[BMIM]Cl solution: complete deformation in the air-gap region. *Cellulose* 22(3):1963–1976. <https://doi.org/10.1007/s10570-015-0613-3>
- Xia X, Wang J, Wang H, Zhang Y (2016) Numerical investigation of spinneret geometric effect on spinning dynamics of dry-jet wet-spinning of cellulose/[BMIM]Cl solution. *J Appl Polym Sci* 133(38):43962. <https://doi.org/10.1002/app.43962>
- Xia XL, Yao YB, Zhu XJ, Mukuze KS, Wang CS, Zhang YM, Wang HP (2014) Simulation on contraction flow of concentrated cellulose/1-butyl-3-methylimidazolium chloride solution through spinneret orifice. *Mater Res Innov* 18(sup2):S874–S878. <https://doi.org/10.1179/1432891714Z.000000000484>

Publisher's Note Springer Nature remains neutral with regard to jurisdictional claims in published maps and institutional affiliations.